pISSN 1229-3008 eISSN 2287-6251
Progress in Superconductivity and Cryogenics
Vol.22, No.3, (2020), pp.7~12 https://doi.org/10.9714/psac.2020.22.3.007

# Interaction of cracks and precipitate particles on the REBCO superconducting layers of practical CC tapes through fractographic observations

**Michael de Leon, Mark A. Diaz, and Hyung-Seop Shin***

*Department of Mechanical Design Engineering, Andong National University, Andong, Kyungbuk, 36729 Korea*

(Received 12 September 2020; revised or reviewed 28 September 2020; accepted 29 September 2020)

**Abstract**

Electromechanical properties of REBCO CC tapes are known to be limited by defects (cracks) that form in the brittle REBCO layer. These defects could be inherently acquired during the CC tapes' manufacturing process, such as slitting, and which can be initiated at the CC tapes' edges. If propagated and long enough, they are believed to cause critical current degradation and can substantially decrease the delamination strength of CC tapes. Currently, commercially available CC tapes from various manufacturers utilize different growth techniques for depositing the REBCO layers on the substrates in their CC tapes preparation. Their epitaxial techniques, unfortunately, cannot perfectly avoid the formation of particles, in which sometimes acts as current blocking defects, known as outgrowths. Collective research regarding the composition, size, and formation of these particles for various CC tapes with different deposition techniques are particularly uncommon in a single study. Most importantly, these particles might interact in one way or another to the existing cracks. Therefore, systematic investigation on the interactions between the cracks' development mechanism and particles on the REBCO superconducting layers of practical CC tapes are of great importance, especially in the design of superconducting devices. Here, a proper etching process was employed for the CC tapes to expose and observe the REBCO layers, clearly. The scanning electron microscope, field emission scanning microscope, and energy-dispersive x-ray spectroscopy were utilized to observe the interactions between cracks and particles in various practical CC tapes. Particle compositions were identified whether as non-superconducting or superconducting and in what manner it interacts with the cracks were studied.

*Keywords*: REBCO coated conductors, precipitate particles, microcracks interaction, scanning electron microscopy, energy-disperse x-ray

## 1. INTRODUCTION

A new frontier in high magnetic field devices and revolutionary power applications have been achieved through the discovery of several cuprate-perovskite ceramic materials which showed superconductivities above the boiling point of liquid nitrogen [1]. Known as second-generation high-temperature superconductors, it uses cuprates of RE-Ba-Cu-O, where RE stands for rare-earth, such as Y, Gd, Sm, etc. Most designs for these superconductors use wires known as coated conductors (CC) which are essentially long lengths of metallic tape with deposited layers of oxide buffer and REBCO. Intrinsically, these CC tapes have superior superconducting properties, such as high critical current characteristics even under high magnetic fields and large current carrying capacity [2].

Currently, several technologies, including ranges of REBCO deposition techniques with optimized epitaxial textured buffer layers at a cost-effective manner, have been pursued by multiple CC tape manufacturers. The biggest blockade, so far, is how to maintain the layer of the reactive and brittle REBCO in lengths with the balance of highly desired aligned crystalline grains and nanostructured defects distributed within the crystalline grains. CC tapes routinely produced around the world were based on the manufacturers' inherent developed growth techniques for depositing the REBCO layer on the CC tapes substrate. However, the intrinsic brittleness of REBCO and various grain misorientation within the layer combined with the process of fabricating the CC tapes, make it susceptible to many current limiting factors. Factors, like cracks created during the slitting process and undesirable a-axis grains, can easily interrupt the superconducting current transport behaviors. Although related topics have been somewhat tackled in various significant studies [3-8], surprisingly, this area is still far from being fully understood.

Therefore, in this study, the mechanism of cracks and its interactions with precipitate particles on the REBCO layers of differently made CC tapes were analyzed and discussed through fractographic observations.

## 2. EXPERIMENTAL PROCEDURES

### 2.1. CC tape samples

Observed samples utilized different growth techniques for depositing the REBCO layers on substrates in CC tapes preparation, as outlined in Table 1. For the Sample 1, IBAD/GdBCO 4-mm wide CC tape, fabricated by the

* Corresponding author: hsshin@anu.ac.kr

TABLE 1
SPECIFICATIONS OF THE CC TAPE SAMPLES.

| | Sample 1 | Sample 2 | Sample 3 | Sample 4 |
|---|---|---|---|---|
| **Fabrication process** | **IBAD/RCE-DR** | **IBAD/MOCVD** | **ISD/RCE** | **IBAD/PLD** |
| **Structure** | Cu stabilized Ag/GdBCO/$LaMnO_3$/ IBAD-MgO/ $Y_2O_3$/$Al_2O_3$/ Stainless steel | Cu-stabilized Ag/YBCO/LaMO Homo-epi MgO/IBAD MgO/Hastelloy | Cu-stabilized Ag/GdBCO/ISD-MgO/Hastelloy | Ag/GdBCO/EuBCO/ MgO/Hastelloy |
| **REBCO film thickness** | ~ 1.5 μm | ~ 1.6 μm | ~3-5 μm | ~4.5 μm |
| **Critical current, $I_c$** | ~250 A | ~110 A | ~184 A | ~190 A |
| **Dimension, *t* x *w*** | 0.144 mm x 4.06 mm | 0.085 mm x 4.06 mm | 0.147 mm x 4.07 mm | 0.126 mm x 4.04 mm |
| **Substrate/ thickness** | ~100 μm | ~50 μm | ~100 μm | ~50 μm |
| **Stabilizer/technique** | Cu electroplated, surround (~15 μm) | Cu electroplated, surround (~20 μm) | Cu electroplated, surround (~43 μm) | Cu electroplated, surround (~20 μm) |

RCE-DR process was used [9]. $LaMnO_3$-buffered IBAD-MgO were used as buffer layers on the templates for the GdBCO layer atop a stainless-steel (STS) substrate. A ~1 μm silver (Ag) layer was used to wrap and protect the GdBCO CC tape. The CC tape was encapsulated with a Cu stabilizer using an electroplating process.

For the Sample 2, 4-mm wide CC tape, architecture was comprised of a superconducting layer, based on the *YBCO*, and fabricated by metal-organic chemical vapor deposition (MOCVD) [10]. Deposition via IBAD or sputtering of a bi-axially textured stack of buffer layers was done atop a Hastelloy substrate and act as a template layer for the introduction of the REBCO material. Lastly, Ag and Cu stabilizers were sputtered and electroplated to the CC tape completely, to provide good electrical contact. Both Sample 1 and Sample 2 CC tapes' substrates were electropolished, as a prerequisite for the successful addition of the buffer layers and superconducting layers. Further, both were produced by slitting the 12-mm-wide one to application-specific tape widths using a double-shearing process and rotary slitters.

For Sample 3, the inclined substrate deposition (ISD) was used. REBCO layer was epitaxially grown on biaxially textured ISD-MgO-buffered and non-magnetic Hastelloy substrate in two steps [11]. First, the MgO buffer layer was textured for substrate deposition at an inclined position resulting in a MgO layer with a roof tile surface structure and a tilt of the main crystallographic axes as well as pronounced biaxial texture. Secondly, the texturing of the MgO buffer layer, which was directly optimized for REBCO layer growth. The second thin MgO layer is evaporated onto the ISD layer to facilitate the epitaxial growth of the REBCO. The REBCO is then deposited directly onto this second MgO layer using RCE. Ag surround coating was used for contact layering, followed by Cu surround coating for electrical and mechanical stabilization.

Sample 4 was fabricated by advanced IBAD for biaxially textured buffer layers and a large pulse-laser deposition (PLD) system with hot wall heating for depositing the REBCO layer [12]. The supplied sample was also surrounded by Ag and Cu as protection layers.

Unlike with Sample 1 and Sample 2 CC tapes where cracks can be initiated by the slitting process and can be generated evenly at the edges [4,13], both the supplied Sample 3 and Sample 4 are free from slitting during the fabrication processes. Since sample slitting cannot be performed in our lab, artificial striation was adopted and made at the center part of the samples, instead. After cleaning the samples' surfaces with acetone followed with alcohol, striation was made at the surface facing the REBCO layer at the desired length. A Sharp-tip cutter was used with moderate pressure, enough to cut the REBCO thru the buffer layers.

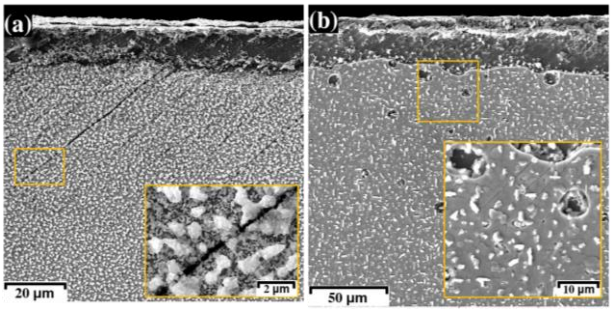

Fig. 1. REBCO surface morphology along the edge of (a) Sample 1 GdBCO and (b) Sample 2 YBCO CC tapes.

2.2. Surface crack morphology observation

The suitable etching process for four different REBCO CC tapes was carefully selected. All samples have Ag surround coatings sputtered after REBCO deposition to provide electrical contact and Cu electroplating that surrounds the tape. The Cu and Ag layers should be removed properly by etching for clear REBCO layer observation: to etch the Cu layer, the sample was immersed in the solution of 30% vol. $HNO_3$ + 70% vol. $H_2O$ for 2 mins or more, depending on the thickness of Cu surround. To etch the Ag, the sample was immersed in the solution of 25% vol. $H_2O_2$ + 25% vol. $NH_4OH$ + 50% vol. $H_20$ for 10 s soaking time. Each sample was rinsed with water after each etching procedure and dry in air. The surfaces of the REBCO layers were imaged using field emission scanning microscope (FE-SEM), and energy-dispersive x-ray spectroscopy (EDS) to investigate the microcracks mechanism and to identify the phase composition of local areas within the REBCO layers.

## 3. RESULTS AND DISCUSSION

3.1. REBCO surface morphology

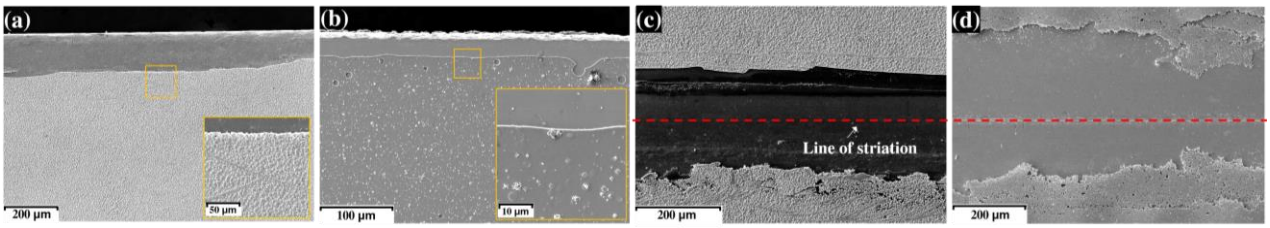


Fig. 2. Surface morphology of REBCO layers along the edges of as received 4-mm CC tapes (a) Sample 3 and (b) Sample 4. Images of REBCO layers' surfaces along the center part of the striated (c) Sample 3 and (d) Sample 4 CC tapes.

Observation of etched surfaces revealed the morphologies of exposed REBCO layers obtained using FE-SEM. As-received 4-mm wide samples from Sample 1 and Sample 2 were shown in Fig. 1. Aside from both were subjected to the slitting process, no strain or any processing other than etching was applied to either tape. As can be seen in the images, REBCO layers at edges were partly removed, with visible cracks originated from the edge and propagated inward. Cracks were more pronounced in Sample 1 with an average length of ~60 µm and were distributed randomly along the edge with an inclined orientation, while void-like defects are distinct in Sample 2. Voids might be related to Cu-rich surface particles defect distributed throughout the REBCO layer [13]. The application of chemical etching presumably led to the removal of concentrated Cu along with the REBCO layer, which created voids. Precipitate particles at various structures and sizes are also present on the REBCO surfaces. At scale-in images, most cracks were observed in transgranular fracture patterns, in which cracks presumably grow and propagate through the precipitate particles. These particles can be non- or superconducting particles and will be discussed in subsequent sections. Nevertheless, the observed cracks, voids, and particles that appeared due to different fabrication process variables are considered current limiting factors in causing non-uniformity properties in REBCO CC tapes [14].

Figures 2 (a) and (b) show the surface morphologies along the edges of as-received etched Sample 3 and Sample 4, respectively. No noticeable cracks were present near the CC tapes' edges, aside from the non-uniform growth or deformation of REBCO layers. Both have empty layers of REBCO along the edges with ~200 µm for the Sample 3 and ~50 µm for the Sample 4. Particles dominantly observed in Samples 1 and 2 are also lacking (scale-in images).

The samples with artificially fabricated striation at the center of the 4-mm samples are presented in Fig. 2 (c) and (d). Portions of the REBCO layer near or at the line of striation were no longer observed, roughly 200 µm at both sides of striation for Sample 3 (Fig. 2 (c)). Some REBCO layers along the edge were deformed, while in most parts, no cracks were visible nor created by the striation process (like the as-received sample). It is assumed, however, that portions of the REBCO layer were pushed, deformed, and delaminated together with the protective layers of Ag and Cu during the striation process and consequently removed during etching. On the other hand, the striated Sample 4 in Fig. 2 (d) produced visible REBCO layer delamination

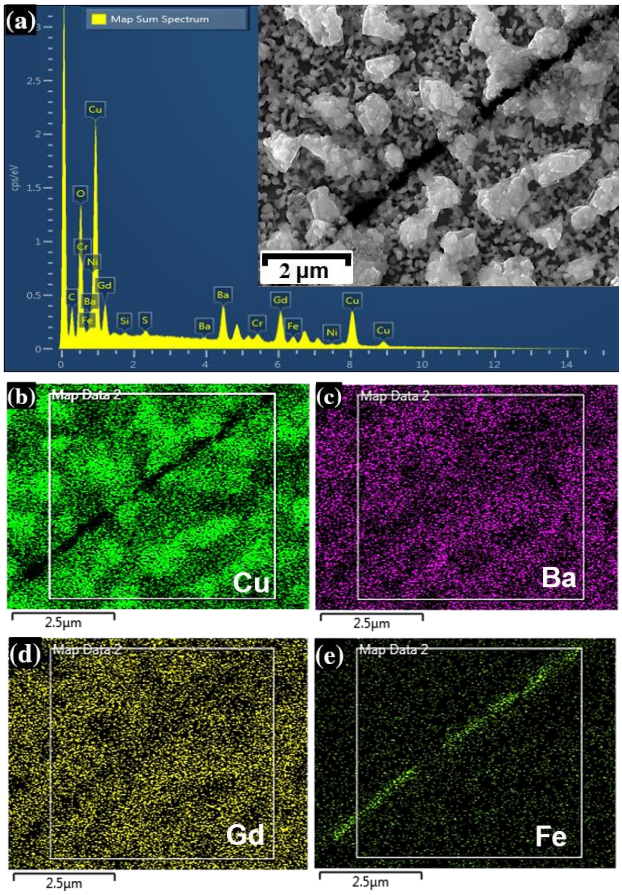


Fig. 3. (a) SEM micrograph with map sum spectrum of Sample 1 etched surface. Mapped elements concentration for (b) Cu, (c) Ba, (d) Gd, and (e) Fe.

from both sides of the striation line. A delaminated REBCO layer was observed, covering nearly 300 µm from line of striation to REBCO layer edge. Cracks were in various lengths and sizes and propagated in random directions, but all initiated at the location of striations. The damage induced in the REBCO layer by the striation was severe and extended to the Hastelloy substrate of the tape (more details are discussed in the mapped elements of the succeeding section). The delamination density due to the interfacial debonding of the layers was also high and found extended inward. The presence of a few particles is visible, with cracks randomly propagates along and through it.

### 3.2. Identification of precipitate particles

At higher magnification, cracks and particles observed

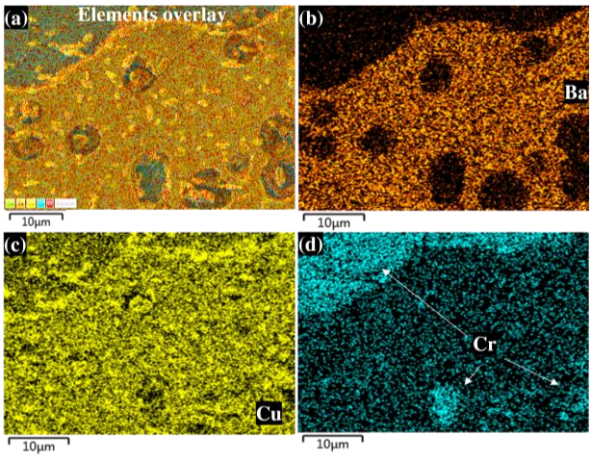


Fig. 4. (a) Elements overlay image for Sample 2. Mapped elements concentration for (b) Ba, (c) Cu, and (d) Cr.

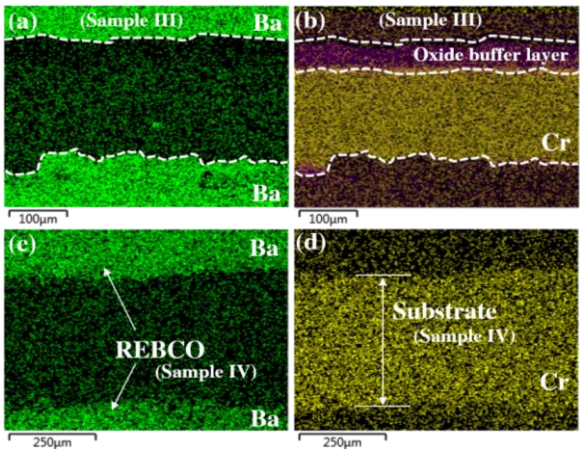


Fig. 5. Mapped elements concentration for Sample 3 (a) Ba and (b) Cr, and Sample 4 (c) Ba and (d) Cr.

through SEM and mapped using EDS for the Sample 1 were presented in Fig. 3 (a) to (e). Randomly distributed particles observed near and surrounding the crack are dominantly composed of Cu and O, as non-superconducting particles, while Ba and Gd were observed around it, as shown in Fig. 3 (c) and (d). The substrate layer was also observed visible within the crack, Fig. 3 (e). Quantitatively, Cu and O elements were present at wt. % of nearly 31 and 18, respectively, while Gd and Ba were 34% and 14%, respectively, as can be seen in the map spectrum in Fig. 3 (a). As for the pinpoint spectrum, one single particle is nearly 54% composed of Cu and 21% O while Gd and Ba are both < 5%.

Sample 2 with the YBCO layer was observed and mapped in Fig. 4 (a) to (d). Overlay image in Fig. 4 (a) detailed the distribution of Ba, Cu, and Cr. The concentration of Ba was observed surrounding the bigger particles enclosed by voids (Fig. 4 (b)), while Cu was abundantly scattered at bigger and smaller particles (Fig. 4 (c)). The Cr which represents the substrate layer was also visible from the edge of the Ba and in some voids, see Fig. 4 (d). The voids that are presumably created by bigger particles which then exposed the Hastelloy substrate are considered substantial in REBCO layer delamination. This indicates that the observed precipitate particles are potentially one of the significant current limiting factors that can strongly depress $I_c$ and $J_c$.

Unlike Samples 1 and 2, Samples 3 and 4 have no distinct randomly oriented precipitate particles. Likewise, no cracks other than the striation cracks were observed on the surfaces of the REBCO layers, exclusively in Sample 4. Nevertheless, the length of the delaminated REBCO part in Sample 3 is doubled in Sample 4 (Fig. 5 (a) to (d)). The mapped elements of Samples 3 and 4 in Fig. 5 (a) to (d) and in the SEM images in Fig. 2 (c) to (d) show that layers of flaked elements were delaminated randomly. A layer of oxide buffer was also exposed in Fig. 5 (b). These resemble that cracks may be formed first at the substrate or buffer layers before it propagates and delaminated the REBCO layer.

### 3.3. Interaction behavior of cracks and precipitate particles

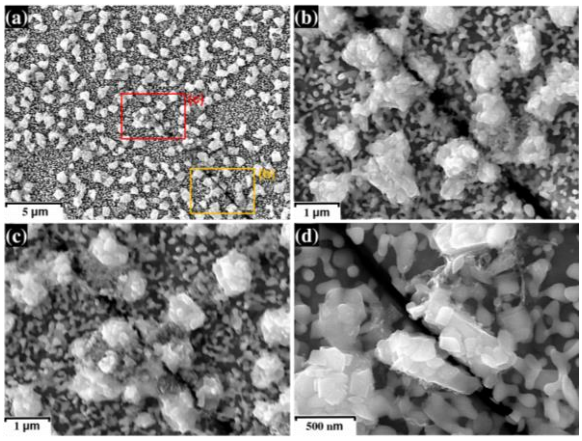


Fig. 6. (a) SEM image of etched Sample 1, showing the interaction between particles and crack at various locations, (b) to (c). (d) another image of crack and particle interaction interaction.

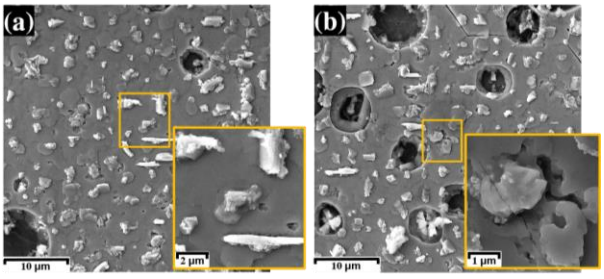


Fig. 7. SEM images of etched Sample 2 revealing a (a) needle-liked particle and (b) cracks through particles.

The propagation of cracks and their interaction with particles were observed and shown in Fig. 6 for Sample 1. It is noted that the observed crack is located at the other edge of the tape, opposite to the image presented in Fig. 1 (a). Eventually, the crack grows in an inclined direction from the edge of the tape with particles directly at its path. By looking closely at the magnified images in Fig. 6 (b), (c), and (d), the crack propagates through the dominantly larger particles, resembling a transgranular fracture before

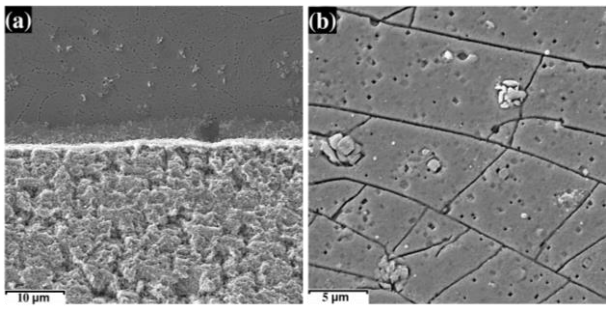


Fig. 8. Surface images showing (a) oriented shaped surface for Sample 3 and (b) cracks branching for Sample 4.

it pinned and disappeared. While smaller size grain/particle encouraged the transgranular cracking in theory [15], bigger particles deeply embedded within the REBCO layer may also cause great strain localization. Similarly, a recent study in YBCO CC tape reported that cracks propagating from bottom to top of the REBCO layer tend to propagate first near the particles before moving to the thickness direction of the YBCO layer [7]. This can be supported by the image in Fig. 3 (e), in which the crack exposed the substrate layer of the tape.

The exposed REBCO surface of Sample 2 revealed the existence of needle-liked particles with an average length of 5 μm (Fig. 7 (a)). They are known as a-axis particles since their c-axes are ~90˚ misoriented from the normal REBCO film and are commonly penetrated through the full thickness of the REBCO layer [14]. These particles were deposited when the REBCO deposition temperature was low and considered as a current-limiting defect [16-17]. In Fig. 7 (b), aside from particle transgranular cracking, a crack was also observed altering its original propagation direction and then propagates again along the particle's boundary.

The majority of edges in Sample 3, which uses the ISD/RCE process did not develop significant cracks on the REBCO layer (Fig. 8 (a)), even after the introduction of artificial striation. The typical tilted epitaxial growth orientation of the REBCO layer, perpendicular to the tape direction was also observed. On the contrary, Sample 4 was observed with different crack propagation modes, with cracks generally originating at the striated edge and propagated inward (Fig. 8 (b)). Rarely seen particles were also observed deflecting the cracks toward multiple directions before branching-out, while some were pinned. Interestingly, the point spectra of the said particles are mainly composed of Ba and Gd with randomly scattered Cu. Presumably, the precipitate particles' growth may be limited only above the REBCO layer.

With different REBCO layer deposition techniques, commercially available practical CC tapes showed that cracks and precipitate particles can be developed differently. Some are vulnerable to REBCO layer cracking even during the manufacturing process, while others have resistance. Precipitate particles composed mainly of Cu and O frequently have cracks extended through-out the thickness of the REBCO layer, and normally represented by transgranular cracking. Shallow particles, on the other hand, developed multiple modes of crack propagation which might be beneficial in the long term and under various load conditions since it can increase the fracture toughness. Aside from these observations, other factors that are not included here, such as thermal coefficient expansion analysis, applied stress effects, *etc.*, all those that may greatly contribute to the cracks and precipitate particle interactions are mostly needed in future studies.

## 4. SUMMARY

REBCO layers of four differently made practical CC tapes were fractographically observed. After chemical etching, to remove the CC tapes' protective layers, the interaction mechanisms between cracks and precipitate particles were analyzed. The results show that the presence of current limiting factors, such as cracks propagated through particles, are abundantly distributed, especially for Samples 1 and 2. With the artificially imposed REBCO layer slitting through striation, such as in Samples 3 and 4, the delamination of the REBCO layer was pronounced. Different modes of crack propagation with particles' interaction are also randomly present, which might interact in one way or another in the long-term CC tapes' device applications. Generally, the different deposition techniques currently employed by several CC tapes' manufacturers should be further optimized to allow significant CC tapes' performance enhancement.

## ACKNOWLEDGMENT

This work was supported by a research Grant of Andong National University.

## REFERENCES

[1] K. Muller and J. Bednorz, "Possible high Tc superconductivity in the Ba-La-Cu-O system", *Phys. B*, vol. 64, pp. 189-193, 1986.
[2] M. Oomen, "AC loss in superconducting tapes and cables", Dissertation, University of Twente, 2020.
[3] H-S. Shin, M. de Leon, and M.A. Diaz, "Investigation of the electromechanical behaviors in Cu-stabilized GdBCO coated conductor tapes using high-cycle fatigue tests at 77 K and related fractographic observations", *Supercond. Sci. Technol.*, vol. 33, pp. 025012, 2020.
[4] A. Gorospe, M. Dedicatoria, and H-S. Shin, "Influence of edge geometry on the delamination strength of REBCO CC tapes using anvil test method", *IEEE Trans.Appl. Supercond*, vol. 26, pp. 1-5, 2016.
[5] H-S. Shin, "Evaluation of delamination characteristics in GdBCO CC tapes under transverse load using anvil test methods for various anvil contact configurations at 77 K", *Supercond. Sci. Technol.*, vol. 32, pp. 104001, 2019.
[6] M. de Leon and H-S. Shin, "Reliability evaluation procedure of electromechanical properties in GdBCO CC tapes obtained by uniaxial tension and fatigue tests at 77 K", *IEEE Trans.Appl. Supercond*, vol. 30, pp. 1-5, June 2020.
[7] L. Shen, C. Liu, and X. Zhang, "Rules of non-superconducting phase particles on crack propagation in YBCO coated conductors fabricated by the IBAD-MOCVD", *Supercond. Sci. Technol.*, vol. 33, pp. 105007, 2020
[8] S. Rogers, W. Chan, and J. Schwartz, "Effects of room-temperature

tensile fatigue on critical current and n-value of IBAD–MOCVD YBa2Cu3O7-x/Hastelloy coated conductor", *Supercond. Sci. Technol.*, vol. 29, pp. 085013, 2016.

[9] J. Lee, *et.al.*, "RDE-DR, a novel process for coated conductor fabrication with high performance," *Supercond. Sci. Technol.*, vol. 27, pp. 044018, 2014.

[10] SuperPower-inc, retrieved: September 10, 2020. http://www.superpower-inc.com

[11] THEVA Pro-Line, retrieved: September 10, 2020. 2020. www.theva.com

[12] Fujikura Ltd, retrieved: September 10, 2020. www.fujikura.co.uk.

[13] S. Rogers and J. Schwartz, "Tensile fatigue behavior and crack growth in GdBa2Cu3O7−x/stainless-steel coated conductor grown via reactive co-evaporation", *Supercond. Sci. Technol.*, vol. 30, pp. 045013, 2017.

[14] P. Li P, *et.al.*, "Observation of important current-limiting defects in a recent high pinning force MOCVD IBAD-MgO coated conductor", *Supercond. Sci. Technol.*, vol. 25, pp. 025002, 2012.

[15] F. Liang and C. Laird, "Control of intergranular fatigue cracking by slip homogeneity in copper I: Effect of grain size", *Mat. Sci. Eng. A*, vol.117, pp. 95–102, 1989.

[16] M. Solovyov, *et.al.*, "Non-uniformity of coated conductor tapes" *Supercond. Sci. Technol.*, vol. 26, pp. 115013, 2013

[17] G. Li, et.al., "Precisely determined temperature window size for the growth of high-quality c-axis oriented YBCO films by photo-assisted MOCVD", *Physica C*, vol. 468, pp. 2213-2218, 2008.